Intermetallics 90 (2017) 180–187

Contents lists available at ScienceDirect

Intermetallics

journal homepage: www.elsevier.com/locate/intermet

Creep of binary Fe-Al alloys with ultrafine lamellar microstructures

A. Schmitt[a,*], K.S. Kumar[b], A. Kauffmann[a], X. Li[c], F. Stein[c], M. Heilmaier[a]

[a] Institute for Applied Materials (IAM), Karlsruhe Institute of Technology (KIT), Karlsruhe, Germany
[b] School of Engineering, Brown University, Providence, RI, USA
[c] Structure and Nano-/Micromechanics of Materials, Max-Planck-Institut für Eisenforschung GmbH, Düsseldorf, Germany

ARTICLE INFO

Keywords:
A. Aluminides
B. Creep
C. Casting
F. Electron microscopy
Scanning
G. Automotive uses

ABSTRACT

On the Al-rich side of the Fe-Al binary system, the eutectoid decomposition of Fe_5Al_8 into B2-ordered FeAl and triclinic $FeAl_2$ in the composition range of 55–65 at.% Al produces an ultrafine lamellar microstructure. The compression creep behavior of such two-phase intermetallic materials was investigated in the temperature range 600–800 °C under constant stress. In addition to the fully lamellar Fe-61Al alloy, Fe-58Al and Fe-62Al that included, pro-eutectoid FeAl and $FeAl_2$, respectively, were characterized in terms of their microstructure and creep response. For all microstructures, the strain rate as a function of time and strain exhibits a distinct minimum instead of a steady state creep regime. Microstructure instability, primarily in the vicinity of colony boundaries, is identified as the main reason for the increase in strain rate beyond the minimum. In contrast, lamellar coarsening is shown to be only a secondary factor influencing creep response for the conditions investigated. In comparison to single phase FeAl, the fully lamellar FeAl-$FeAl_2$ shows enhanced creep resistance while the presence of either pro-eutectoid phase leads to a relative deterioration of the creep resistance.

1. Introduction

Iron aluminides are of interest as an alternative to advanced steels intended for high temperature structural applications. Their excellent intrinsic oxidation resistance [1–3], lower density and material costs make them attractive candidates in potentially replacing steels in some of these applications [4–7]. However, their widespread use is limited mainly due to (i) low ductility at room temperature [8] and (ii) reduced creep resistance at elevated temperatures beyond 600 °C [9–11]. It has been shown that the creep resistance of B2-ordered FeAl can be improved by classical physical metallurgy approaches such as solution strengthening with alloying elements like Ti, Zr, Mo [12–14], precipitation strengthening by addition of C or B which form carbides and borides respectively [12,14] and dispersion strengthening, for instance, using Y_2O_3 nanoparticles [15]. Another strategy for improving creep resistance is to utilize a lamellar microstructure that may be obtained through a eutectic or eutectoid decomposition process. Thus, in the case of TiAl alloys, it has been shown that a fine, lamellar microstructure can substantially improve creep resistance [16].

A lamellar arrangement of two intermetallic phases has been observed in the Fe-Al-system in the composition range 55–65 at.% Al and is based on the eutectoid decomposition of the high-temperature ε-phase Fe_5Al_8 (space group: $I\bar{4}3m$, no. 217; Pearson symbol: $cI52$) [17] into B2-ordered FeAl ($Pm\bar{3}m$, no. 221; $cP2$) and triclinic $FeAl_2$ ($P\bar{1}$, no. 2; $aP19$) [18]. The eutectoid decomposition occurs at 60.9 at.% Al and at 1095 °C [19]. The mechanical properties at high temperature of such in-situ composites in the binary Fe-Al system have not been investigated in detail so far. In the present study, compression creep experiments of eutectoid and off-eutectoid binary compositions were carried out in the temperature range 600–800 °C; the deformed microstructures were examined and correlated with the observed mechanical response.

2. Experimental

The materials were produced by arc melting pieces of pure Al (99.99%) and Fe (99.99%). The chamber was purged with Ar and evacuated multiple times in an effort to reduce the oxygen partial pressure, and the final pressure in the chamber was maintained at 60 kPa. Additionally, a lump of Zr metal was melted in the chamber prior to melting the Fe-Al alloys to further reduce residual oxygen. The Fe-Al buttons were flipped and re-melted five times to ensure homogenization. Final rods with dimensions of 14 mm diameter and 170 mm length were achieved by drop casting into a water-cooled Cu mold.

Three two-phase alloy compositions corresponding to Fe-58Al, Fe-61Al and Fe-62Al (at. %) and single-phase, stoichiometric Fe-50Al were produced. Fe-61Al is expected to result in a fully lamellar microstructure according to the published binary phase diagram [19] whereas Fe-58Al and Fe-62Al contain a significant fraction of pro-

* Corresponding author.
E-mail address: anke.schmitt@kit.edu (A. Schmitt).

http://dx.doi.org/10.1016/j.intermet.2017.07.016
Received 4 May 2017; Received in revised form 5 July 2017; Accepted 20 July 2017
Available online 01 August 2017

eutectoid FeAl and $FeAl_2$ respectively. Additionally, a single-phase $FeAl_2$ composition was prepared by levitation melting; this specimen in the as-cast state is not single-phase because $FeAl_2$ does not form congruently from the melt and instead a non-equilibrium microstructure results in the as-cast state [19]. Thus, it requires a subsequent long-term heat-treatment to produce the single-phase. The as-cast microstructures were investigated using scanning electron microscopy (SEM). The samples were prepared by standard metallographic procedures including mechanical grinding followed by polishing with 1 μm diamond suspension. Final polishing was performed using a non-crystallizing oxide polishing suspension OP-S provided by Buehler, Illinois, USA. The average lamellar spacing was measured in the as-cast state for all three alloys and in the eutectoid alloy after exposure to 700 °C for various times, and after creep testing. The experimental approach to determine lamellar spacing is described elsewhere [20]. The volume fraction of the pro-eutectoid phase was evaluated utilizing imaging analysis software (AnalySis).

Cylindrical samples with a diameter of 5 mm and a height of 8 mm were electrical discharge machined for creep experiments. The samples were isothermally crept in compression, either at constant true stress in vacuum, or at constant load in air. It is noted that for small strains (for example, ≤ 10%), no difference can be discerned between constant true stress and constant load curves. The tests were carried out in the temperature range between 600 and 800 °C and the applied stress was varied from 50 to 175 MPa.

3. Results and discussion

3.1. Initial microstructure

In the as-cast state, all three two-phase alloys exhibit a lamellar arrangement of FeAl and $FeAl_2$ and include morphological irregularities like terminations and branches (Fig. 1a–c). In the off-eutectoid Fe-58Al and Fe-62Al alloys, in addition to the lamellar morphology composed of FeAl and $FeAl_2$, pro-eutectoid FeAl and $FeAl_2$ are observed respectively. Average lamellar spacing and the associated standard deviations were determined in the as-cast state for the three alloys and are summarized in Table 1. The experimentally measured volume fractions of the pro-eutectoid phases are included in Table 1 and match reasonably well with the values calculated using the binary phase diagram in Ref. [19].

3.2. Creep behavior of the fully lamellar material

The creep response (at 700 °C and a nominal constant stress of 100 MPa) for the eutectoid alloy with the lamellar microstructure is shown in Fig. 2a and b. The data are shown as logarithm of strain rate versus strain in Fig. 2a, and as logarithm of strain rate versus time in Fig. 2b. The resulting creep curve does not exhibit a “classical” steady-state regime of constant strain rate over a measurable period of strain or time. Instead, a characteristic minimum occurs, which is dependent on temperature and stress (these relations are presented later in Figs. 8 and 9). After passing through the minimum, the strain rate markedly increases with increasing time and strain at 700 °C (Fig. 2a and b).

The increase in the creep rate beyond the minimum for the eutectoid alloy presented above is thought to be a result of microstructural changes along the lines of previous reports in the literature [21,22]. We note here that a similar creep response was also observed for the off-eutectoid two-phase alloys. Common to all three alloys is the presence of a rather large fraction of the lamellar microstructure and changes associated with it are believed to be responsible for the increase in strain rate beyond the minimum. In general, the strength and creep resistance at high temperature of lamellar materials strongly depend on the lamellar spacing [23,24], and on the lamellar orientation with respect to the loading axis [25]. Lamellar orientation to the loading axis is of minor importance in the present case since polycrystalline, non-textured as-cast alloys are being investigated. An increase in lamellar spacing can lead to a decrease in high temperature strength and creep resistance by at least three distinct microscopic mechanisms [24]: a) lamellar coarsening enables a longer dislocation glide distance within a lamella, b) the shear stress to bow out dislocations trapped at the interface decreases with increasing lamellar spacing [26], and c) the ability to operate Frank-Read sources is easier in coarser lamellae. Coarsening of a lamellar microstructure can be continuous or discontinuous depending on the test temperature and applied stress. For example, in the case of fully lamellar Ti-Al alloys, discontinuous coarsening of the lamellar microstructure is observed at lower stress levels [27], whereas at higher stresses, deformation-induced spheroidization occurs [28]. In both cases, the deterioration in the lamellar microstructure is reported to be the major reason for an increase in creep rate.

Thus, the evolution of lamellar spacing as a function of time and strain in the Fe-61Al alloy was determined by measuring the average lamellar spacing, λ, after various times of thermal exposure and mechanical loading, respectively. An increase in average lamellar spacing was recognized and confirms that coarsening takes place during creep (Table 2).

In order to separate the effect of thermal and mechanical loading on the coarsening behavior, a heat treatment at 700 °C without applied stress was carried out as well. The resulting change in average lamellar spacing as a consequence of thermal exposure alone is plotted as a function of time using filled symbols in Fig. 3. In order to compare the long term (up to 5000 h) coarsening behavior due to thermal exposure with the data of the creep experiment (open symbols in Fig. 3) a double logarithmic plot was used. The coarsening behavior of lamellar structures has been studied in Refs. [29–31] and is driven by a reduction of total interfacial energy by one or more of several mechanisms including: a) spheroidization [32,33], b) cylinderization [32,33], c)

Table 1
Microstructure data in the as-cast state.

Composition	lamellar spacing/nm	Pro-eutectoid phase	Measured volume fraction of pro-eutectoid particles/vol.%	Calculated volume fraction of pro-eutectoid particles/vol.%
Fe-58Al	400 ± 50	FeAl	31 ± 4	30
Fe-61Al	380 ± 40	–	–	–
Fe-62Al	400 ± 90	$FeAl_2$	33 ± 5	28

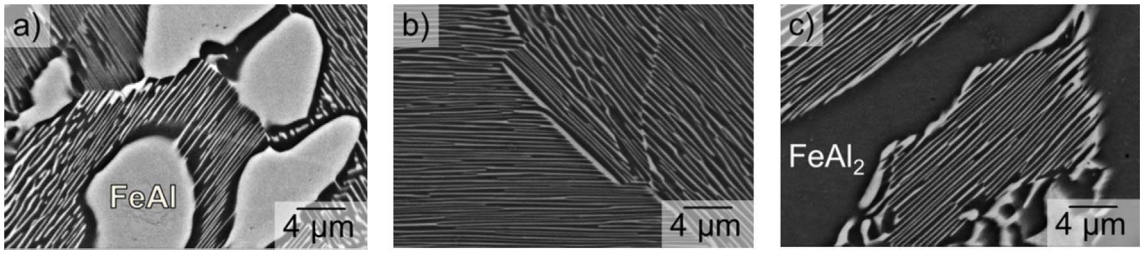

Fig. 1. Backscattered electron images of the two-phase alloys in the as-cast state: a) Fe-58Al, b) fully lamellar Fe-61Al and c) Fe-62Al.

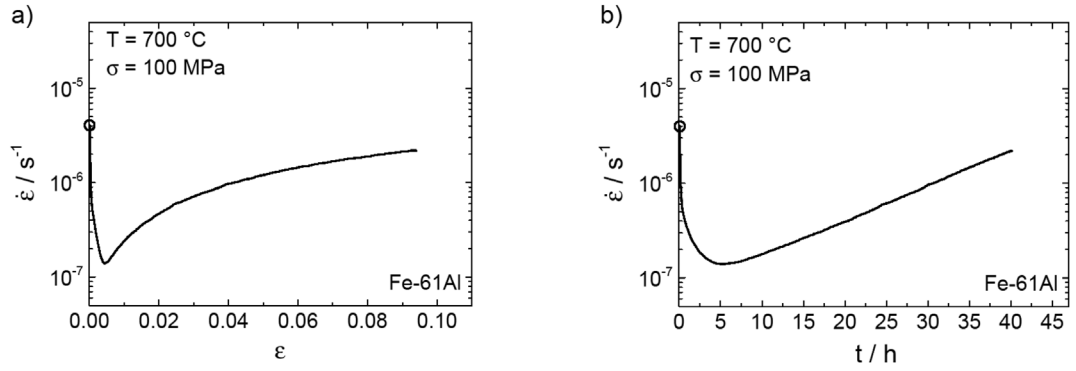

Fig. 2. Creep response of the lamellar Fe-61Al alloy at 700 °C and an applied stress of 100 MPa: a) log strain rate vs. strain and b) log strain rate vs. time. The circles indicate the initial strain rate.

Table 2
Evolution of average lamellar spacing at 700 °C at an applied stress of 100 MPa for the fully lamellar Fe-61Al alloy.

condition	time/h	strain	lamellar spacing λ/nm
as-cast	–	–	380 ± 40
T = 700 °C	5	0.01	390 ± 70
σ = 100 MPa	30	0.05	520 ± 70
	50	0.20	680 ± 110

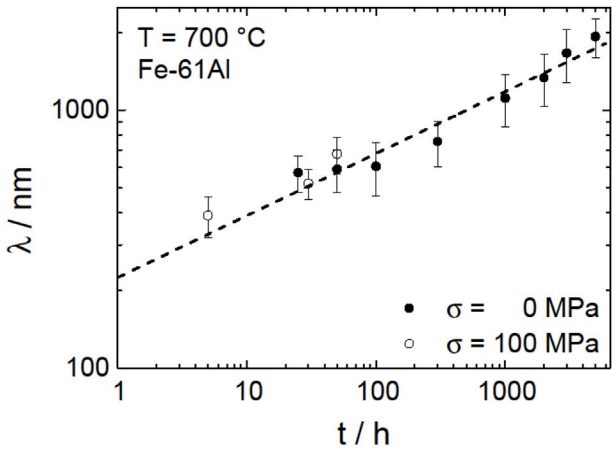

Fig. 3. Change in average lamellar spacing with time at 700 °C with (open symbols) and without (filled symbols) an applied stress of 100 MPa for the fully lamellar Fe-61Al. The dashed line helps to visualize that coarsening response during creep is comparable to that for the heat treated material.

thermal grooving [34] and/or d) termination/migration [35]. A recent detailed study of the coarsening of lamellar FeAl and $FeAl_2$ [36] confirmed that the process is volume diffusion-controlled and follows a classical ripening law as

$$\lambda^3 = \lambda_0^3 + kt \quad (1)$$

where λ is the average lamellar spacing, λ_0 the initial average lamellar spacing and k a constant. The superposition of stress on the coarsening response does not appear to influence the observed trend for times up to 50 h as shown by the open symbols in Fig. 3. Hence, we conclude that in the regimes of temperature and stress examined in this study, coarsening of the lamellae is mainly a consequence of thermal exposure during creep.

To investigate the effect of increased lamellar spacing on creep behavior, a previously heat-treated sample (700 °C for 300 h) with a coarser average lamellar spacing of 760 ± 150 nm was tested. Fig. 4a compares the creep behavior of this sample with that for the as-cast material with a finer average lamellar spacing of 380 ± 40 nm. A careful examination of Fig. 4a confirms that in the early stages of the experiment (roughly within the first percent of strain), the heat-treated microstructure creeps at a faster rate than does the as-cast material; however, at larger strains (and beyond the minimum in creep rate in Fig. 4a), the creep rates converge and the effect of lamellar spacing on creep rate gradually diminishes. This suggests that changes in average lamellar spacing due to coarsening are unlikely to be the primary cause for the degradation in creep response beyond the minimum creep rate noted in Fig. 4a.

An additional experiment was conducted to more vividly demonstrate that increases in average lamellar spacing only have marginal (if any) influence on the accelerated creep response beyond the minimum creep rate. We used a single specimen that was initially in the as-cast state, to eliminate inevitable variations in the initial microstructure when multiple specimens are used. Here, the sample was first loaded at 700 °C and 100 MPa and allowed to reach the minimum strain rate of $2 \times 10^{-7}\,s^{-1}$ (Fig. 4b) which is in good agreement with the minimum strain rate previously observed in the as-cast condition in Fig. 2a. The sample was then unloaded and allowed to isothermally coarsen for 20 h at this test temperature (note that the total plastic strain at the minimum strain rate is small and will not affect the coarsening rate appreciably). Following that, it was reloaded to 100 MPa and strain evolution was again monitored as a function of time. The results are shown for this second step in Fig. 4b as well. A second minimum is noted beyond which the strain rate increases again. The occurrence of a minimum in the second loading step is puzzling. It suggests that during the isothermal coarsening, the structure must have recovered and subsequent loading enables it to harden. However, considering that the measured global plastic strain is less than one percent at the minimum strain rate (Fig. 4a), this is unlikely unless there is significant plastic strain partitioning between the two phases - i.e. one phase plastically deforms in the early stages while the other is elastic and the plastically deforming phase recovers during the intermittent anneal; this hypothesis remains to be verified.

Returning to Fig. 4b, a dashed line is incorporated that depicts what should have happened if the initial loading had not been interrupted at the minimum strain rate and creep had continued in accordance with Fig. 2b. The 20 h exposure to 700 °C following the initial loading should result in an average lamellar spacing of the order of ~520 nm (Fig. 3) as compared to 379 nm for the as-cast condition. If coarsening was the decisive factor controlling strain rate evolution beyond the minimum, reloading should result in a strain rate evolution that is coincident with this extrapolation.

The second minimum, however, is observed at $4 \cdot 10^{-7}\,s^{-1}$ which is significantly lower than the value predicted by the dashed curve (about $1.5 \cdot 10^{-6}\,s^{-1}$). Subsequent increase in strain rate with time beyond this minimum parallels the extrapolated dashed line. For these reasons, the change in lamellar spacing cannot be the primary reason for the experimentally observed increase in strain rate beyond the minimum

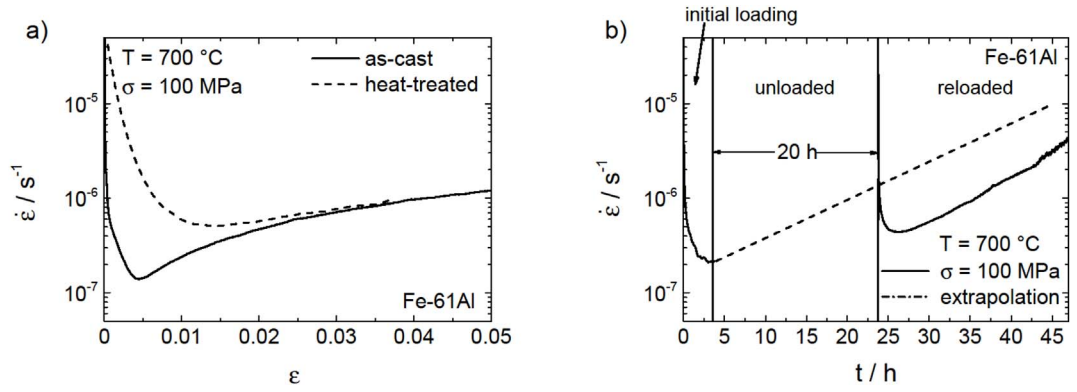

Fig. 4. The effect of changing the lamellar spacing on creep response under constant true stress: a) comparison of an as-cast specimen (solid line) with a specimen initially heat-treated at 700 °C for 300 h (dashed line) to alter the lamellar spacing; b) a single specimen that was initially in the as-cast state and was crept to the minimum, then unloaded and in-situ coarsened for 20 h and then subsequently reloaded.

strain rate in Fig. 2a and b as well as in Fig. 4a.

Since lamellar coarsening has been ruled out as the primary cause of the increased creep rate beyond the minimum in Fig. 4a and b, it is necessary to consider other aspects of microstructural degradation. Previous work on the creep of lamellar TiAl has shown that the fine structure of colony boundaries can control creep resistance. Specifically, smooth colony boundaries can lead to colony boundary sliding [37] and crack growth [38] whereas interlocking boundaries have been shown to promote a distinct steady-state regime [39] and, thus, to enhance creep resistance [37]. In the lamellar Fe-Al alloys examined in this study, the microstructure in the vicinity of colony boundaries in the as-cast state reveals various “irregularities” relative to the periodicity exhibited within the colonies; in some instances, the minor phase in the lamellar structure displays terminations short of reaching the boundary (Fig. 5b), leaving a 1–5 μm region of single phase layer of the majority phase, while at other boundaries, the lamellar morphology in the adjacent colonies extends right up to the colony boundary but the lamellae themselves are mismatched across the boundary (Fig. 5c). Furthermore, along some colony boundaries but not others, FeAl precipitates are present as stringers (Fig. 5b).

Microstructure degradation during creep in these colony boundary regions is accelerated compared to the interior due to stress incompatibilities, elastic anisotropy and lamella terminations. Thus, subsequent to creep exposure of 50 h at 700 °C at a constant stress of 100 MPa (this corresponds to a global plastic strain of about 0.2), the scale of microstructure and microstructural morphology in the vicinity of the colony boundaries has significantly changed as compared to the colony interior and as depicted in Fig. 5d (white arrows indicate one such region). A region of 10–20 μm width is present in the vicinity of colony boundaries where the lamellar structure is no longer evident but is replaced by enlarged single–phase regions of FeAl and $FeAl_2$. If we argue that this microstructural degradation in the vicinity of colony boundary contributes to the enhanced creep rate, then it follows that $FeAl_2$ likely contributes to high temperature creep deformation, implying that this phase with its triclinic crystal structure experiences plastic flow at 700 °C. Anyway, it would be unrealistic to observe a plastic strain of 0.2 without any plastic flow of the $FeAl_2$ phase that constitutes about 70 vol.% of the present large colony size material. In a detailed crystallographic study presented elsewhere [40], it was shown that the (114)[1$\bar{1}$0], ($\bar{1}\bar{1}$3)[1$\bar{1}$0] and (221)[1$\bar{1}$0] of $FeAl_2$ exhibit similar atomic arrangement to the {1$\bar{1}$0}001 slip system in B2 FeAl [41] and it seems reasonable to assume that slip occurs on these systems in $FeAl_2$ at elevated temperatures; however, this remains to be verified. Hence, we hypothesize that one of the two phases deforms plastically in the early state of creep whereas the minimum in creep rate could signal the onset of plastic deformation of the second phase; plastic co-deformation of the two phases can subsequently lead to a progressive loss in microstructure stability by dynamic recovery/recrystallization of the

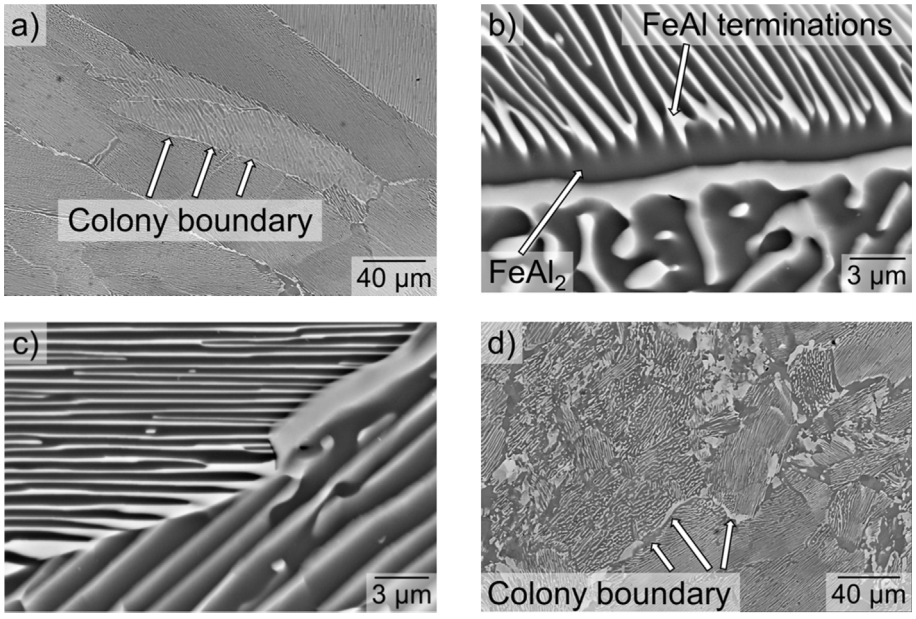

Fig. 5. BSE micrographs of the fully lamellar Fe-61Al alloy in the (a–c) as-cast condition: (a) general microstructure, and (b,c) higher magnification images showing FeAl lamellae terminating short of the colony boundary in (b) and FeAl lamellae mismatch across colony boundary in (c). (d) Microstructure coarsening at colony boundaries after 50 h of creep at 700 °C and 100 MPa.

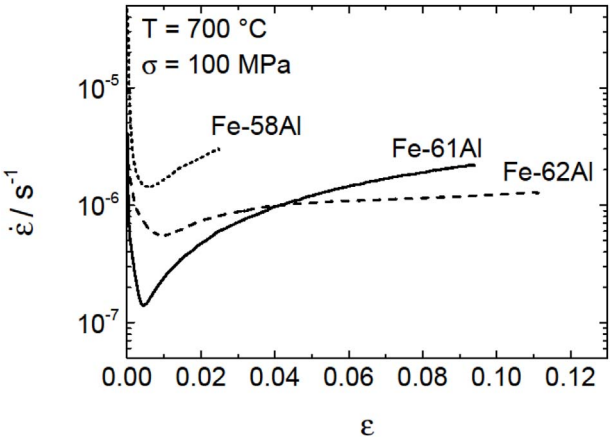

Fig. 6. A comparison of the creep response of Fe-58Al, Fe-61-Al and Fe-62Al alloys at 700 °C and an applied true stress of 100 MPa.

individual phases, more so in the vicinity of colony boundaries but to a lesser extent within the colony themselves leading to an increase in strain rate. If this is the case, then, it implies that changes in creep mechanism during the course of the constant stress experiment can cause significant difficulties in the interpretation of the experimentally determined activation energy for creep.

3.3. A comparison of the creep response of Fe-58Al, Fe-61Al and Fe-62Al

The effect of the presence of pro-eutectoid FeAl or $FeAl_2$ in a lamellar FeAl/$FeAl_2$ matrix on creep response is illustrated in Fig. 6 along with the behavior of the eutectoid alloy. Again, the comparison is made at 700 °C and 100 MPa and all creep curves show a pronounced minimum in creep rate. The fully lamellar alloy exhibits the lowest minimum strain rate of the three alloys. It appears that the presence of the globular pro-eutectoid FeAl or $FeAl_2$ phases (and a corresponding reduced amount of the lamellar eutectoid) leads to a deterioration in creep resistance. Further, beyond the strain rate minimum, the increase in creep rate with strain is affected by the presence and type of pro-eutectoid phase. Whereas the increase for the fully lamellar Fe-61Al alloy and the aluminum-lean Fe-58Al alloy run almost parallel to each other, the aluminum-rich Fe-62Al exhibits a more gradual change intersecting the curve for the Fe-61Al alloy at a strain of ~0.04 (Fig. 6) and thereafter improved creep resistance relative to the eutectoid alloy is noted. This response may be related to the fact that $FeAl_2$ is more creep resistant than FeAl (see Fig. 7).

To further explore this line of thinking, creep tests under similar

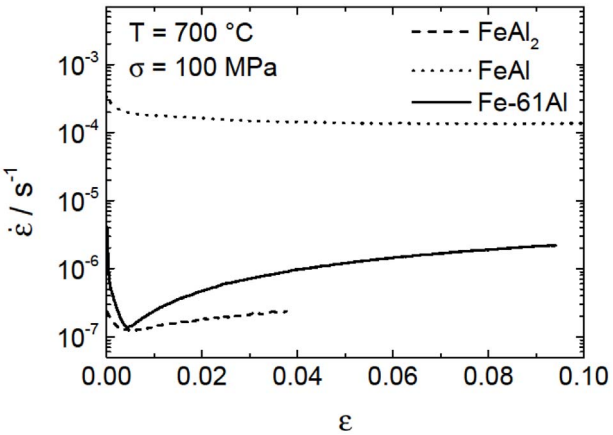

Fig. 7. Creep response of single-phase stoichiometric FeAl and $FeAl_2$ compared to fully lamellar, two-phase Fe-61Al at 700 °C and an applied true stress of 100 MPa.

conditions (100 MPa; 700 °C) were performed on single phase stoichiometric FeAl and single phase $FeAl_2$ specimens and the results are compared in Fig. 7 against the response of the fully lamellar Fe-61Al eutectoid alloy. In Fig. 7, the minimum strain rate for $FeAl_2$ (dashed line) is comparable to the one for the fully lamellar material (continuous curve). Post-deformation examination of the crept $FeAl_2$ specimens showed that on a macroscopic scale, they had deformed homogeneously despite the presence of minor levels of porosity. The creep resistance of $FeAl_2$ is clearly superior to that of stoichiometric FeAl (dotted line) (note: The composition of FeAl in equilibrium with $FeAl_2$ at 700 °C is only slightly Al-rich compared to stoichiometric FeAl) but the presence of a fine lamellar structure is morphologically beneficial for creep in that the creep of the weaker phase (FeAl) is constrained by the more creep-resistant $FeAl_2$ phase in the early stages of creep. In this sense, a fully lamellar microstructure provides optimum creep resistance as was previously observed for TiAl as well [16]. However, for longer exposure times, and beyond the creep rate minimum, when lamellae degradation particularly in the vicinity of the colony boundaries commences, the volume fraction of the more creep-resistant $FeAl_2$ phase (pro-eutectoid globules) can become rate-controlling as seen in Fig. 6.

3.4. Rate controlling creep mechanism and activation energy

Based on the above results, the creep response of these three two-phase Fe-Al alloys can be separated into two parts: 1) creep until the minimum strain rate which was reached at a strain less than one percent, and 2) creep beyond the minimum and up to strains as large as 20% that was reached in about 50 h, at which point, the eutectoid lamellar morphology in the vicinity of colony boundaries appeared to have deteriorated (Fig. 5d). To correctly interpret the measured creep exponents and activation energies from these experiments, it is important to understand the dominant deformation mode(s) through the duration of such experiments. For example, a) both phases may contribute to the creep deformation from the beginning and it is the degradation of the lamellar morphology that is responsible for the increase in the strain rate beyond the minimum; b) only one of the two phases deforms and the second phase does not contribute directly to creep throughout the entire experiment, and the degradation of the lamellae causes the increase of the strain rate beyond the minimum, or c) the second phase starts to creep-deform beyond the minimum causing the increase in the strain rate and subsequently, lamellar degradation enters the picture as well.

Since the creep strain at which the minimum creep rate occurs is less than one percent, it is conceivable that this relatively small global plastic strain can be accommodated predominantly within one phase with little or no permanent deformation of the second phase. This implies that cases b) and c) described above are possible. The FeAl phase is significantly less creep-resistant than the $FeAl_2$ phase as presented in Fig. 7. If it is assumed that until the strain rate minimum is reached, the plastic deformation is only supported by FeAl, then a change in the stress exponent as well as in the activation energy would be expected beyond the minimum.

We now consider the minimum strain rate (≤one percent of plastic strain) and the strain rate at a plastic strain of 0.04. The second value was chosen since the increase in the strain rate beyond the minimum diminishes after a strain in the range of 0.02–0.04 (Fig. 7); thereafter, to a first approximation, it is viewed as approaching a steady-state regime. The stress dependence of the minimum strain rate (filled circles in Fig. 8) as well as the strain rate at a strain of 0.04 (open circles in Fig. 8) at 700 °C for different imposed stress levels is summarized in a Norton plot as a double logarithmic representation of strain rate versus stress (Fig. 8). The power law stress exponent was determined according to:

$$\dot{\varepsilon} = A \cdot \sigma^n \tag{2}$$

where $\dot{\varepsilon}$ is the strain rate, A is a temperature-dependent constant and σ

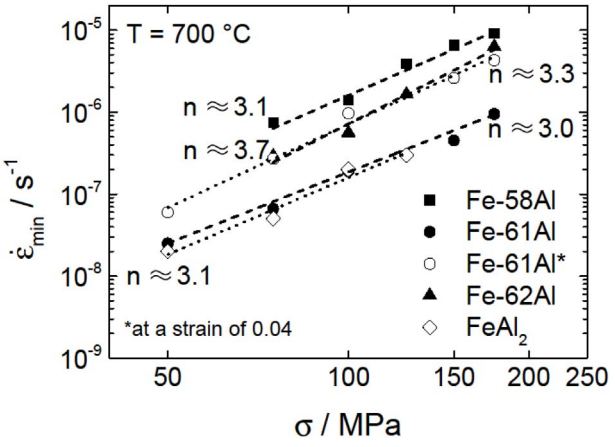

Fig. 8. Stress dependence of the minimum strain rate at 700 °C for the three two-phase alloys and for single-phase $FeAl_2$. In addition, the stress dependence of the strain rate at a strain of 0.04 is also included for the Fe-61Al alloy (open circles). The stress exponent n is in the range 3–4 in all cases.

is the applied stress. The resulting stress exponent n is 3.0 for the minimum creep rate and 3.3 for the strain rate at a strain of 0.04. A stress exponent between 3 and 5 in a single-phase alloy typically signifies that creep (rate) is controlled by thermally activated dislocation glide and climb [42,43]. However, in this study, we are dealing with a two-phase lamellar microstructure where it is uncertain if both phases are experiencing permanent deformation or if one phase deforms only elastically, and also whether the response remains the same at the minimum strain rate and at the strain rate at a strain of 0.04. It is also important to know the creep characteristics of the individual phases and how they work together in a fine lamellar structure that includes a high density of interfaces.

In previous studies on FeAl single-phase material, a stress exponent of 3.5 was obtained for deformation in the temperature range of 600 °C–1000 °C and at applied stresses between 50 and 200 MPa [44]. The operative slip systems in this temperature range were determined to be $\{1\bar{1}0\}001$ and $\{100\}001$ [41]. The stress exponent obtained in this study for single-phase $FeAl_2$ (open rhombi in Fig. 8) is 3.1 and also indicative of dislocation glide/climb dominated creep. As both of these phases that constitute the eutectoid microstructure deform by dislocation-mediated creep under the imposed temperature and stress regime, it is difficult from the stress exponent value alone to determine whether one or both phases is/are responsible for creep at the minimum strain rate or at the strain rate at a strain of 0.04.

When creep is climb-controlled, vacancy diffusion kinetics influence the creep rate, and thus, an examination of the activation energies could provide additional information on the operating mechanism. In order to determine the activation energy, creep experiments were carried out at different temperatures at a constant stress level of 100 MPa. The minimum strain rates obtained are plotted as a function of inverse temperature in Fig. 9 for the eutectoid and off-eutectoid alloys together with the strain rates determined at a plastic strain of 0.04 for the eutectoid composition. The values for the activation energy obtained from the slopes of these Arrhenius plots for the fully lamellar Fe-61Al alloy are (321 ± 26) kJ/mol and (338 ± 21) kJ/mol for the minimum strain rate and the strain rate at a strain of 0.04 respectively. Both these values are above those reported in the literature by Eggersmann et al. [45,46], for self-diffusion of Fe (265 kJ/mol), as well as for diffusion of In and Zn in B2-ordered Fe-50Al (258 kJ/mol); In and Zn are the usual substitutes for Al due to the lack of suitable Al tracers [45]. The values provided by Eggersmann [45,46], are also supported by Nakamura et al. [47] for off-stoichiometric Fe-48Al of 250 kJ/mol for Fe- and 249 kJ/mol for Al-diffusion using single phase diffusion couples. Additionally, the coarsening behavior of a fully lamellar FeAl/$FeAl_2$ material has been characterized with an activation energy of 265 kJ/mol [36]. Thus, while coarsening itself occurs during creep, it does not appear to be the rate determining factor. The additional stress that is applied in creep activates other processes which are responsible for creep deformation.

In contrast to the above discussion, reported values in the literature for activation energy for creep of B2-ordered Fe-(39–49)Al of 460 kJ/mol by Whittenberger [48] and 395 kJ/mol by Jimenez & Frommeyer [44] are significantly higher than the values for self-diffusion but no clear explanation has been provided for this remarkable difference. It is worth noting that the diffusion data were collected in the temperature range of 500–1200 °C whereas creep data were only generated between 600 and 800 °C and therefore it is not clear whether the degree of disorder and/or the types of complex aggregates of point defects may have influenced the reported activation energy values. Thus, according to the phase diagram from Kubaschewski [49] a transition from α_2(l) to α_2(h) occurs at ~ 800 °C in stoichiometric B2, a phenomenon that was originally reported by Köster and Gödecke [50]. Other studies [51,52] have examined the nature of point defects and their mobility in FeAl alloys and claim that for Al concentration greater than 35 at.% in FeAl, triple defect aggregates have to be considered in the α_2(l) region whereas in the α_2(h) regime, additional di-vacancies are formed.

The activation energy for creep of single-phase $FeAl_2$ and the activation energies for self-diffusion of Fe and Al in $FeAl_2$ are not readily available in literature. For this reason, the activation energy for creep of single phase $FeAl_2$ was characterized in this investigation in the temperature range 650 °C–800 °C at a nominal stress level of 100 MPa and found to be 309 ± 83 kJ/mol (see Fig. 9b). This value matches well with the values obtained for the dual phase material, confirming that the creep behavior is primarily determined by the more creep resistant $FeAl_2$ phase.

Returning to Fig. 8, the minimum strain rate for different stress levels can be used to compare the creep behavior at 700 °C of the three two-phase Fe-Al alloys (Fe-58Al, Fe-61Al and Fe-62Al) and of the single-phase $FeAl_2$ material against each other. The stress exponent is in the range of 3–4 for all cases. Observations that can be made from Fig. 8 for all stress levels examined include: (i) the Fe-58Al alloy containing FeAl as the pro-eutectoid phase is the least creep resistant, (ii) Fe-62Al containing $FeAl_2$ as the pro-eutectoid phase is better but not as good as the fully lamellar Fe-61Al alloy, and (iii) single phase $FeAl_2$ is superior in creep response (as measured using the minimum creep rate) relative to the off-eutectoid alloys but the response of the fully lamellar alloy virtually overlaps the behavior of single phase $FeAl_2$. If we assume that both phases in fully lamellar Fe-61Al deform plastically at the minimum, then from the results from Figs. 7–9, we can conclude that creep under these conditions in the fully lamellar alloy is dominated by the $FeAl_2$ phase.

With respect to activation energy for creep (as determined using the minimum strain rate), it can be seen in Fig. 9 that for all examined alloys at a stress of 100 MPa and in the temperature interval of 600 and 800 °C, the activation energies lie in a narrow range between 309 and 321 kJ/mol.

4. Conclusions

The compressive creep behavior of a fully lamellar eutectoid Fe-61Al alloy as well as off-eutectoid Fe-58Al and Fe-62Al alloys that contain pro-eutectoid FeAl and $FeAl_2$, respectively, was examined at elevated temperatures. The main findings include:

- Creep rate as a function of time/strain exhibits a distinct minimum; a steady state creep regime does not occur.
- Lamellar coarsening observed during creep is primarily attributed to thermal exposure; the contribution from imposed mechanical loads is secondary. Lamellar coarsening within the colony only plays a minor role in affecting the creep response beyond the observed minimum of the creep rate.

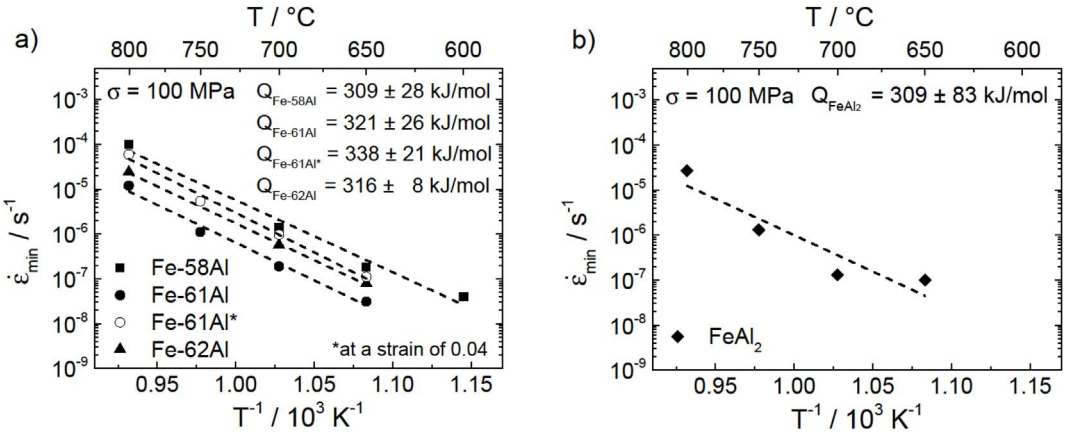

Fig. 9. Arrhenius plot for the three alloys showing the variation in minimum strain rate with test temperature at a fixed stress level of 100 MPa. From these data, activation energy for creep was calculated. a) For all investigated two-phase alloys; the variation of strain rate at a strain of 0.04 with temperature for the eutectoid alloy is also included; b) for the $FeAl_2$ single phase.

- The morphological instability of the lamellar microstructure, particularly in the vicinity of colony boundaries during creep is identified as the main reason for the observed increase in strain rate beyond the minimum.
- The presence of a pro-eutectoid phase (FeAl or $FeAl_2$) leads to a deterioration in the creep resistance. By comparing the creep response of the FeAl/$FeAl_2$ lamellar eutectoid microstructure with that for single phase FeAl and $FeAl_2$, it is shown that the lamellar arrangement significantly enhances the creep resistance at least until the minimum creep rate is attained.
- The stress exponent at 700 °C for these two-phase alloys was determined to be 3–4 in all cases examined; while in a single-phase solid solution, this would signify creep controlled by dislocation glide and climb, a mechanism-based explanation for this observation in these multiphase lamellar alloys requires detailed microscopy analysis of the deformed structures and this work is in progress.
- The activation energy of 309–321 kJ/mol is higher than those reported for self-diffusion in FeAl but lower than the ones reported for creep of stoichiometric and near stoichiometric FeAl.
- The results from the Norton plot and the experimentally determined activation energy strongly indicate that beyond the strain rate minimum both phases deforms and contribute to the creep behavior but $FeAl_2$ is the rate controlling phase.

Acknowledgement

The authors gratefully acknowledge funding by the German Research Foundation (DFG) within the project “Fein-lamellare Fe-Al in-situ Kompositwerkstoffe” (HE 1872/26-1). This work was additionally supported by the Karlsruhe House of Young Scientists (KHYS, http://www.khys.kit.edu/) and the Karlsruhe Nano Micro Facility (KNMF, http://www.knmf.kit.edu/), a Helmholtz Research Infrastructure at Karlsruhe Institute of Technology (KIT). M. Heilmaier and K.S. Kumar thank the Alexander von Humboldt Foundation for enabling this international collaboration through a Humboldt Award. A. Kauffmann thanks the Carl-Zeiss-Foundation for financial support in the form of a postdoctoral grant. Thanks are due to M. Palm for fruitful discussions.

References

[1] R. Prescott, M.J. Graham, The oxidation of iron-aluminum alloys, Oxid. Met. 38 (1992) 73–87, http://dx.doi.org/10.1007/BF00665045.
[2] H.J. Grabke, Oxidation of NiAl and FeAl, Intermetallics 7 (1999) 1153–1158, http://dx.doi.org/10.1016/S0966-9795(99)00037-0.
[3] H.J. Grabke, Oxidation of aluminides, Mater. Sci. Forum 251–254 (1997) 149–162 doi:10.4028/ www.scientific.net/MSF.251-254.149.
[4] N.S. Stoloff, Iron aluminides: present status and future prospects, Mater. Sci. Eng. A 258 (1998) 1–14, http://dx.doi.org/10.1016/S0921-5093(98)00909-5.
[5] N.S. Stoloff, C.T. Liu, S.C. Deevi, Emerging applications of intermetallics, Intermetallics 8 (2000) 1313–1320, http://dx.doi.org/10.1016/S0966-9795(00)00077-7.
[6] M. Palm, Fe–Al materials for structural applications at high temperatures: current research at MPIE, Int. J. Mater. Res. 100 (2009) 277–287, http://dx.doi.org/10.3139/146.110056.
[7] C.T. Liu, K.S. Kumar, Ordered intermetallic alloys, part I: nickel and iron aluminides, JOM 45 (1993) 38–44, http://dx.doi.org/10.1007/BF03223218.
[8] C.T. Liu, J. Stringer, J.N. Mundy, L.L. Horton, P. Angelini, Ordered intermetallic alloys: an assessment, Intermetallics 5 (1997) 579–596, http://dx.doi.org/10.1016/S0966-9795(97)00045-9.
[9] K. Yoshimi, S. Hanada, M.H. Yoo, On lattice defects and strength anomaly of B2-type FeAl, Intermetallics 4 (1996) S159–S169, http://dx.doi.org/10.1016/0966-9795(96)80194-4.
[10] I. Baker, P.R. Munroe, Mechanical properties of FeAl, Int. Mater. Rev. 42 (1997) 181–205, http://dx.doi.org/10.1179/imr.1997.42.5.181.
[11] E.P. George, I. Baker, Thermal vacancies and the yield anomaly of FeAl, Intermetallics 6 (1998) 759–763, http://dx.doi.org/10.1016/S0966-9795(98)00063-6.
[12] W.J. Zhang, R.S. Sundar, S.C. Deevi, Improvement of the creep resistance of FeAl-based alloys, Intermetallics 12 (2004) 893–897, http://dx.doi.org/10.1016/j.intermet.2004.02.020.
[13] F. Dobeš, P. Kratochvíl, The effect of Zr addition on creep of Fe-30 at.% Al alloys, Intermetallics 43 (2013) 142–146, http://dx.doi.org/10.1016/j.intermet.2013.07.017.
[14] R.S. Sundar, S.C. Deevi, High-temperature strength and creep resistance of FeAl, Mater. Sci. Eng. A 357 (2003) 124–133, http://dx.doi.org/10.1016/S0921-5093(03)00261-2.
[15] D.G. Morris, I. Gutierrez-Urrutia, M.A. Muñoz-Morris, High temperature creep behaviour of an FeAl intermetallic strengthened by nanoscale oxide particles, Int. J. Plast. 24 (2008) 1205–1223, http://dx.doi.org/10.1016/j.ijplas.2007.09.001.
[16] S. Huang, Microstructures and property tradeoffs in wrought tial-base alloys, Metall. Trans. Phys. Metall. Mater. Sci. 23 (1992) 375–377, http://dx.doi.org/10.1007/BF02660879.
[17] F. Stein, S.C. Vogel, M. Eumann, M. Palm, Determination of the crystal structure of the epsilon phase in the Fe-Al system by high-temperature neutron diffraction, Intermetallics 18 (2010) 150–156, http://dx.doi.org/10.1016/j.intermet.2009.07.006.
[18] I. Chumak, K.W. Richter, H. Ehrenberg, Redetermination of iron dialuminide, $FeAl_2$, Acta Crystallogr. Sect. C-Cryst. Struct. Commun. 66 (2010) 87–88, http://dx.doi.org/10.1107/S0108270110033202.
[19] X. Li, A. Scherf, M. Heilmaier, F. Stein, The Al-Rich part of the Fe-Al phase diagram, J. Phase Equilibria Diffus. 37 (2016) 162–173, http://dx.doi.org/10.1007/s11669-015-0446-7.
[20] A. Scherf, D. Janda, M.B. Yazdi, X. Li, F. Stein, M. Heilmaier, Oxidation behavior of binary aluminium-rich Fe-Al alloys with a fine-scaled, lamellar microstructure, Oxid. Met. 83 (2015) 559–574, http://dx.doi.org/10.1007/s11085-015-9535-6.
[21] H. Mughrabi, U. Tetzlaff, Microstructure and high-temperature strength of monocrystalline nickel-base superalloys, Adv. Eng. Mater. 2 (2000) 319–326, http://dx.doi.org/10.1002/1527-2648(200006)2:6<319::AID-ADEM319>3.0.CO;2-S.
[22] J. Albiez, I. Sprenger, C. Seemüller, D. Weygand, M. Heilmaier, T. Böhlke, Physically motivated model for creep of directionally solidified eutectics evaluated for the intermetallic NiAl–9Mo, Acta Mater. 110 (2016) 377–385, http://dx.doi.org/10.1016/j.actamat.2016.02.024.
[23] P.D. Crofts, P. Bowen, I.P. Jones, The effect of lamella thickness on the creep behaviour of Ti-48Al-2Nb-2Mn, Scr. Mater. 35 (1996) 1391–1396, http://dx.doi.org/10.1016/S1359-6462(96)00323-5.
[24] C.E. Wen, K. Yasue, J.G. Lin, Y.G. Zhang, C.Q. Chen, The effect of lamellar spacing

on the creep behavior of a fully lamellar TiAl alloy, Intermetallics 8 (2000) 525–529, http://dx.doi.org/10.1016/S0966-9795(99)00131-4.
[25] N. Shiratori, S. Hirata, T. Asai, M. Takeyama, T. Matsuo, Creep and evolution of dynamic recrystallization in single crystals of Ti-48at%Al with different orientation between stress Axis and γ lamellar plate, Key Eng. Mater. 171–174 (2000) 639–646 doi:10.4028/ www.scientific.net/KEM.171-174.639.
[26] F. Appel, R. Wagner, Microstructure and deformation of two-phase γ-titanium aluminides, Mater. Sci. Eng. R. Rep. 22 (1998) 187–268, http://dx.doi.org/10.1016/S0927-796X(97)00018-1.
[27] R. Yamamoto, K. Mizoguchi, G. Wegmann, K. Maruyama, Effects of discontinuour coarsening of lamellae on creep strength of fully lamellar TiAl alloys, Intermetallics 6 (1998) 699–702, http://dx.doi.org/10.1016/S0966-9795(98)00053-3.
[28] J.A. Wert, M.F. Bartholomeusz, Effect of creep strain on microstructural stability and creep resistance of a TiAl/Ti_3Al lamellar alloy, Metall. Mater. Trans. A 27 (1996) 127–134, http://dx.doi.org/10.1007/BF02647753.
[29] H. Cline, Shape instabilities of eutectic composites at elevated temperatures, Acta Metall. 19 (1971) 481–490, http://dx.doi.org/10.1016/0001-6160(71)90002-2.
[30] G. Sharma, R.V. Ramanujan, G.P. Tiwari, Instability mechanisms in lamellar microstructures, Acta Mater. 48 (2000) 875–889, http://dx.doi.org/10.1016/S1359-6454(99)00378-X.
[31] E. Ho, G. Weatherly, Interface diffusion in the Al-$CuAl_2$ eutectic, Acta Metall. 23 (1975) 1451–1460, http://dx.doi.org/10.1016/0001-6160(75)90154-6.
[32] J.C.M. Kampe, T.H. Courtney, Y. Leng, Shape instabilities of plate-like structures—I. Experimental observations in heavily cold worked in situ composites, Acta Metall. 37 (1989) 1735–1745, http://dx.doi.org/10.1016/0001-6160(89)90059-X.
[33] T.H. Courtney, J.C.M. Kampe, Shape instabilities of plate-like structures—II. analysis, Acta Metall. 37 (1989) 1747–1758, http://dx.doi.org/10.1016/0001-6160(89)90060-6.
[34] W.W. Mullins, Theory of thermal grooving, J. Appl. Phys. 28 (1957) 333–339, http://dx.doi.org/10.1063/1.1722742.
[35] L.Y. Lin, T.H. Courtney, K.M. Ralls, Deformation induced microstructural instability in the PbSn eutectic, Acta Metall. 25 (1977) 99–106, http://dx.doi.org/10.1016/0001-6160(77)90113-4.
[36] X. Li, F. Bottler, R. Spatschek, A. Schmitt, M. Heilmaier, F. Stein, Coarsening kinetics of lamellar microstructures: experiments and simulations on a fully-lamellar Fe-Al in situ composite, Acta Mater. 127 (2017) 230–243, http://dx.doi.org/10.1016/j.actamat.2017.01.041.
[37] H. Zhu, D. Seo, K. Maruyama, P. Au, Grain boundary morphology and its effect on creep of TiAl alloys, Mater. Trans. 45 (2004) 3343–3348, http://dx.doi.org/10.2320/matertrans.45.3343.
[38] W.R. Chen, J. Triantafillou, J. Beddoes, L. Zhao, Effect of fully lamellar morphology on creep of a near γ-TiAl intermetallic, Intermetallics 7 (1999) 171–178, http://dx.doi.org/10.1016/S0966-9795(98)00019-3.
[39] R.W. Hayes, B. London, On the creep deformation of a cast near gamma TiAl alloy Ti-48Al-1Nb, Acta Metall. Mater. 40 (1992) 2167–2175, http://dx.doi.org/10.1016/0956-7151(92)90134-Z.
[40] A. Scherf, A. Kauffmann, S. Kauffmann-Weiss, T. Scherer, X. Li, F. Stein, M. Heilmaier, Orientation relationship of eutectoid FeAl and $FeAl_2$, J. Appl. Crystallogr. 49 (2016) 442–449.
[41] Y. Umakoshi, M. Yamaguchi, Deformation of FeAl single-crystals at high-temperatures, Philos. Mag. Phys. Condens. Matter Struct. Defects Mech. Prop. 41 (1980) 573–588.
[42] P. Yavari, T.G. Langdon, An examination of the breakdown in creep by viscous glide in solid solution alloys at high stress levels, Acta Metall. 30 (1982) 2181–2196, http://dx.doi.org/10.1016/0001-6160(82)90139-0.
[43] O.D. Sherby, P.M. Burke, Mechanical behavior of crystalline solids at elevated temperature, Prog. Mater. Sci. 13 (1968) 323–390, http://dx.doi.org/10.1016/0079-6425(68)90024-8.
[44] J.A. Jimenez, G. Frommeyer, Creep behavior of intermetallic Fe-Al and Fe-Al-Cr alloys, Mater. Sci. Eng. Struct. Mater. Prop. Microstruct. Process 220 (1996) 93–99, http://dx.doi.org/10.1016/S0921-5093(96)10480-9.
[45] M. Eggersmann, H. Mehrer, Diffusion in intermetallic phases of the Fe-Al system, Philos. Mag. A 80 (2000) 1219–1244, http://dx.doi.org/10.1080/01418610008212112.
[46] M. Eggersmann, B. Sepiol, G. Vogl, H. Mehrer, Self-diffusion of Fe in iron-aluminides studied by tracer and Mossbauer techniques, Defect Diffus. Forum 143 (1997) 339–344.
[47] R. Nakamura, K. Takasawa, Y. Yamazaki, Y. Iijima, Single-phase interdiffusion in the B2 type intermetallic compounds NiAl, CoAl and FeAl, Intermetallics 10 (2002) 195–204, http://dx.doi.org/10.1016/S0966-9795(01)00125-X.
[48] J.D. Whittenberger, The influence of grain size and composition on slow plastic flow in FeAl between 1100 and 1400 K, Mater. Sci. Eng. 77 (1986) 103–113, http://dx.doi.org/10.1016/0025-5416(86)90358-7.
[49] O. Kubaschewski von Goldbeck, IRON—Binary Phase Diagrams, Springer, Berlin, Heidelberg, 1982, http://dx.doi.org/10.1007/978-3-662-08024-5.
[50] W. Köster, T. Gödecke, Physical measurements on Iron-Aluminum-alloys between 10 and 50 at percent Al .1. confirmation of and additional contribution to the Iron-Aluminum phase-diagram, Z. Met. 71 (1980) 765–769.
[51] R. Kerl, J. Wolff, T. Hehenkamp, Equilibrium vacancy concentrations in FeAl and FeSi investigated with an absolute technique, Intermetallics 7 (1999) 301–308, http://dx.doi.org/10.1016/S0966-9795(98)00118-6.
[52] T. Hehenkamp, P. Scholz, B. Köhler, R. Kerl, Vacancy formation and diffusion in FeAl-alloys, Defect Diffus. Forum 194–199 (2001) 389–396 doi:10.4028/ www.scientific.net/DDF.194-199.389.